RSC Advances

PAPER

View Article Online
View Journal | View Issue

Cite this: *RSC Adv.*, 2014, **4**, 56188

Key aspects of L-threoninium picrate single crystal: an excellent organic nonlinear optical material with a high laser-induced damage threshold

Anuj Krishna,[ab] N. Vijayan,*[b] Shashikant Gupta,[c] Kanika Thukral,[ab] V. Jayaramakrishnan,[d] Budhendra Singh,[e] J. Philip,[f] Subhasis Das,[g] K. K. Maurya[b] and G. Bhagavannarayana[b]

Received 28th August 2014
Accepted 13th October 2014

DOI: 10.1039/c4ra09410g

www.rsc.org/advances

Recent trends focuses on the usage of nonlinear optical materials owing to their increasing demand in frontier areas of optical communication and switching applications. In the present work single crystal of L-threoninium picrate, an excellent material for nonlinear optical applications was grown using conventional slow evaporation solution technique to meet the increasing demand of photonics industry. The lattice parameters of the grown crystal were analysed by using powder X-ray diffraction, and it was found that it crystallised in monoclinic system with space group $P2_1$. The strain in the lattice of the grown crystal was calculated using Hall–Williamson relation. Crystalline perfection of the grown crystal was assessed using high resolution X-ray diffraction technique and observed that quality of crystal was fairly good. Optical transmission analysis and band gap evaluation were performed using UV-Vis spectroscopy. Laser damage threshold value for the crystal was also measured and was found to be higher than most of reported organic single crystals. Optical homogeneity of the crystal and birefringence was evaluated using modified channel spectrum method. Thermal behaviour of the grown specimen was examined by using photopyroelectric technique. Further its various mechanical properties, such as hardness, stiffness, young's modulus, were measured using nanoindentation technique.

1. Introduction

In the contemporary world of information technology, which focuses on fast and high speed data processing, retrieving and transmission[1] has galvanized the young researchers for the search of newer material with enhanced properties for photonics applications. The material to be utilised for nonlinear optical (NLO) applications must be able to alter the amplitude, phase and polarisation of incident laser beam to maximum extent.[2] This extent of alteration is one of the factors that decides the suitability of a material for particular device application. Second harmonic generation (SHG) is one of the most interesting phenomena observed in most of the crystals lacking the centre of symmetry and is widely utilised for applications in optical frequency conversion, optical modulation *etc.* Several crystals, such as β-BaB_2O_4 (BBO),[3] lithium niobate ($LiNbO_3$)[4] and LiB_3O_5 (LBO),[5] owing to their high SHG efficiency and excellent laser damage threshold (LDT) values, are widely employed for NLO applications. However the growth of crystals of the above mentioned materials is a tedious task and requires considerable effort to get defect free crystals. Thus there is a need of a material, which at the same time possesses excellent NLO properties and could easily be grown in the form of single crystals and hence favouring their utilization for photonic applications. Crystals of all amino acids except glycine are good candidates for coherent blue-green laser generation and second harmonic generation applications[6] owing to the presence of chiral carbon atom and non-centrosymmetric crystal structure.[7] These crystals not only possesses good SHG efficiency comparable to the above mentioned materials but also can be easily grown using conventional slow evaporation solution technique (SEST) and thus avoiding the usage of expensive melt growth techniques. Moreover, the greatest advantage in working with amino acids is that their characteristics can be altered and refined using molecular engineering and chemical synthesis.[8] L-Threonine is one of the promising

[a]*Academy of Scientific and Innovative Research, CSIR – National Physical Laboratory, New Delhi-110012, India*

[b]*Council of Scientific and Industrial Research – National Physical Laboratory, New Delhi-110012, India. E-mail: nvijayan@nplindia.org; vjnphy@yahoo.com; Fax: +91-11-45609310; Tel: +91-11-45608263*

[c]*Deenbandhu Chhotu Ram University of Science and Technology, Murthal (Sonepat)-131039, Harayana, India*

[d]*Department of Physics, PSG College of Arts and Science, Coimbatore-641014, Tamilnadu, India*

[e]*TEMA-NRD, Mechanical Engineering Department and Aveiro Institute of Nanotechnology (AIN), University of Aveiro, 3810-193 Aveiro, Portugal*

[f]*Department of Basic Sciences, Amal Jyothi College of Engineering, Kanjirappally, Kottayam 686518, Kerala, India*

[g]*Dept. of Physics, University of Burdwan, Bardhaman, 713-104, India*

amino acids, which has SHG efficiency higher than many of the amino acids.[6] But because of needle like morphology of L-threonine, its employment for NLO applications particularly in designing and development of wave plate became a difficult task. However this drawback of L-threonine can be overcome by synthesising a complex, namely, L-threoninium picrate (LTP), which upon growing into single crystal leads to morphological changes from needle like to rectangular plate like structures thus favouring its usage for designing of wave plates. These complexes of amino acids with picric acid are also found to possess very high SHG efficiency.[9,10] This is because of the presence of highly delocalised π electron system and large extent of charge transfer, due to strong intermolecular interaction (hydrogen bonding) between the donor and acceptor molecule.[11] L-Threoninium picrate (LTP) is one such π donor–acceptor compound, in which L-threonine acts as electron donor and picric acid acts as electron acceptor. Natarajan *et al.*[2] reported a detailed structural and nonlinear optical studies on titled material and showed that both L-threonine and picric acid are connected by strong asymmetric O–H···O hydrogen bond and a N–H···O hydrogen bond and has SHG efficiency 43 times that of KDP, and this value is more than most of amino acids single crystals, such as L-alanine cadmium chloride (LACC),[12] L-arginine hydrochloride monohydrate (LAHCL),[13] L-proline cadmium chloride monohydrate (LPCCM),[14] reported in previously studied reports and hence can be utilized for harmonic generation and optical modulation applications. The main reason explained for this high value of SHG was because of the strong intermolecular interaction between donor (amino group) and acceptor (nitro group), as for a given nitro group maximum efficiency can be obtained by interaction with amino group.[15] However, to the best of our knowledge no systematic studies of LTP have been done till date. Hence, in the present investigation we report for the first time bulk growth, assessment of crystalline perfection, optical, thermal and mechanical properties of LTP single crystal.

2. Experimental

2.1 Synthesis and growth

L-Threoninium picrate (LTP) material was synthesised by taking equimolar ratio of L-threonine and picric acid and then dissolving in double distilled water, which acted as a solvent. Synthesis was performed at a temperature of around 35 °C. The prepared solution was stirred continuously for homogenization for a period of 3 h and then filtered using Whatman paper in order to remove the suspended impurities. The solution was then dried to obtain a white crystalline powder for single crystal growth. The reaction is depicted in Scheme 1. Single crystal growth of titled material was performed using the obtained recrystallised salt, which was taken and dissolved again in double distilled water at a temperature of 30 °C. The beaker containing the solution was then covered with perforated plastic sheet. The beaker was then housed in Eurotherm controlled constant temperature bath (CTB) with an accuracy of ±0.01 °C at 30 °C. Good quality crystals of LTP were obtained from the mother solution after a period of 25 days. Fig. 1 depicts the image of as grown LTP crystal having dimensions 12 × 7 × 2.5 mm^3.

2.2 Characterization techniques

2.2.1 Powder X-ray diffraction. The lattice dimensions of synthesized LTP material was calculated using Rigaku X-ray powder diffractometer. CuKα radiation of wavelength 1.54 Å was used for scanning the sample with a scan rate of 2 degrees per min in the range between 10 to 60 degrees.

2.2.2 High resolution X-ray diffraction. A PANalytical X'Pert PRO MRD high-resolution XRD system, with CuKα_1 radiation, was employed to assess the crystalline perfection of grown crystal. The rocking curves of the crystals for the diffraction planes were recorded in symmetrical Bragg geometry using the natural facets by performing the ω scan[16] with double axis geometry. The monochromated X-ray beam incident on the specimen was obtained using a high-resolution four-bounce Ge(220) monochromator. The diffracted beam from the specimen was detected using a scintillation detector without using any analyzer at the receiving stage (*i.e.* before the detector) to get all the possible information, *e.g.*, the individual peaks from structural grain boundaries, scattered intensity from the dislocations and other defects from the specimen crystal.

2.2.3 Optical transmission analysis. Optical transmission and absorption studies on grown LTP crystal was carried out using SHIMADZU UV-Vis spectrophotometer (Model-1601) in the wavelength region of 200–900 nm. The crystal was cut and polished to thickness of 2 mm and then subjected to spectrophotometer for analysis.

2.2.4 Laser damage threshold analysis. Laser damage threshold value for grown LTP crystal was measured using single shot laser pulses from Nd:YAG laser source with 10 ns pulse width and at 10 Hz repetition rate.[17–19]

2.2.5 Birefringence analysis. Optical homogeneity and birefringence of the crystal was evaluated using modified channel spectrum (MCS) experimental setup, which was based on the principle of channelled spectra. This modification in optics improves the accuracy of the output results. A high power He–Ne laser source was placed at the focal point of CDS collimator lens (focal length ~ 30 mm). In order to get narrow light, an additional pinhole was placed at the focal plane of the eyepiece at the exit side of CDS. Normal incidence was obtained using a method of auto-collimation, where the light (monochromatic light) reflected from the front surface of the crystal was made to fall back on the aperture at the source. The LTP crystal was placed between polarizer and final emerging interference two beam pattern analyzed with CCD camera.

2.2.6 Photopyroelectric technique. The thermal effusivity, diffusivity and conductivity, as well as specific heat capacity of the LTP crystal were measured using photopyroelectric technique, with a 120 mW He–Cd laser of wavelength 442 nm acting as the optical heating source.[20] A sample of LTP crystal in the form of a thin plate, of thickness about one mm, was attached to a thermally thick film of polyvinylidene difluoride (PVDF), which acted as the pyroelectric detector in the experiment.

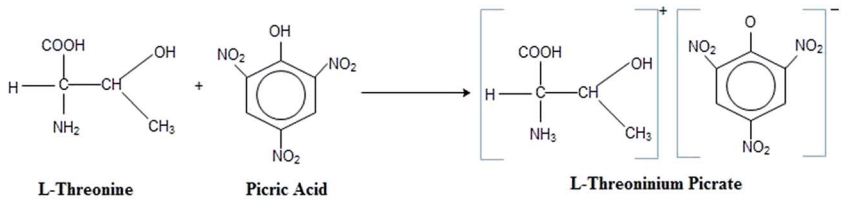

Scheme 1 Reaction Mechanism of LTP.

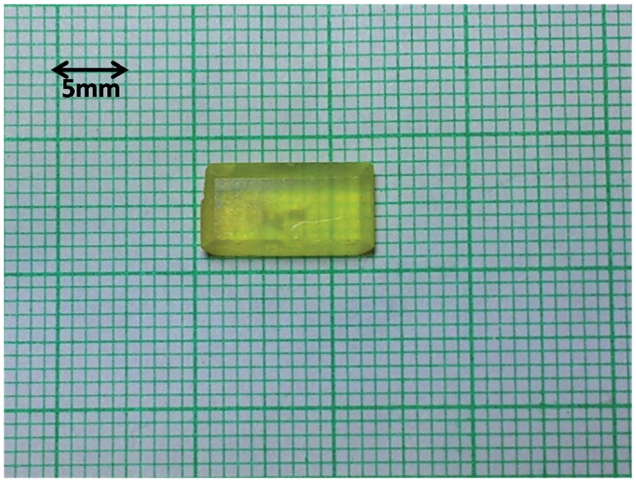

Fig. 1 Photograph of grown LTP single crystal.

The thermal effusivity (e) and diffusivity (α) for LTP crystal were determined from the photopyroelectric (PPE) signal amplitude and phase curves following the procedure described elsewhere.[20] From these values of thermal effusivity (e) and diffusivity (α), specific heat capacity (C_p) and thermal conductivity (k) were calculated.

2.2.7 Nanoindentation analysis. Mechanical properties of the grown crystal were studied using three-sided pyramidal Berkovich diamond indenter owing to its advantage of having sharper tip than four-sided Vickers indenter. Berkovich diamond indenter has an edge radius of 20 nm, and faces at 65.3° from vertical axis which was attached to a fully calibrated nanoindenter (TTX-NHT, CSM Instruments) whose calibration procedures were described elsewhere.[21] Further the indentation impressions were recorded using optical microscope and atomic force microscopy (AFM). The experiment was performed on (−202) plane of LTP crystal with indentation axis normal to it. A total of 6 indenter impressions were made at different places on optically smooth surface of LTP crystal with load ranging from 5–125 mN. The approach speed, dwelling time and load/unload speed was maintained as 2000 nm min^{-1}, 10 s and 20 mN min^{-1}, respectively. The obtained results were analyzed and interpreted using standard Oliver and Pharr method.[22]

The loading and unloading curves were obtained using relation given as,

$$F = \alpha(h - h_f)^m \quad (1)$$

where F is load applied on crystal, α and m are empirical parameters, h is initial displacement and h_f is the final displacement after complete loading and unloading cycle.

From an analysis of unloading response we get an estimate of stiffness and elastic modulus of material. The stiffness $S(dF/dh)$, was evaluated from the initial slope of unloading curve and is given by relation,

$$h_c = h_{max} - \varepsilon \times \frac{F_{max}}{S} \quad (2)$$

where, ε is indenter constant and is equal to 0.75 and h_c is the contact depth and h_{max} is the maximum displacement of the indenter in the crystal with load.

The Young's modulus was also evaluated from the slope of unloading curve, which is given by relation as,

$$E^* = \frac{1}{2}\frac{\sqrt{\pi}}{A}\frac{dF}{dh} \quad (3)$$

The hardness was calculated using the relation,

$$H = \frac{F_{max}}{A_c} \quad (4)$$

where F_{max} is the maximum indentation load and A_c is the projected contact area of indentation.

Further the load -independent hardness (H_0) was evaluated using relation given as,

$$H_0 = ka_2 \quad (5)$$

where k is the constant, which depends on indenter geometry and for three-sided pyramidal Berkovich diamond indenter, which was used in present experiment k is given as 1/24.5. a_2 is the constant evaluated by polynomial fitting of peak load *vs.* contact depth curve.

3. Results & discussions

3.1 Phase and microstrain analysis

Grown crystals of LTP were taken, crushed into fine powder and then subjected to powder X-ray diffractometer for phase analysis. The obtained powder X-ray diffraction pattern is shown in Fig. 2a. The pattern was further analysed using chekcell software and its unit cell dimensions and volume were calculated and compared with reported studies.[2] These dimensions and volume were found to be $a = 9.2482$ Å, $b = 6.2638$ Å, $c = 12.7314$ Å, $\beta = 108.43°$, $V = 699.67$ $Å^3$ and are in good agreement with the reported studies.[2] The obtained pattern clearly shows the

well-defined peaks with high intensity and sharpness, indicating the better crystallinity of the material. This can be understood from the fact that intensity of diffracted X-ray beam depends on the atomic arrangements in the crystal, *i.e.* if the atoms are perfectly arranged in the crystalline material then the interaction between the electrons of atoms present in the material with the X-ray beam would strongly lead to higher intensity of diffracted X-ray beam. The strain (η) in the lattice of as grown crystal was evaluated using Hall–Williamson relation:

$$\beta \cos \theta = K\lambda/\tau + \eta \sin \theta \quad (6)$$

where β, θ, K, λ and τ are full-width half-maxima (FWHM) of diffraction peak, Bragg diffraction angle of the peak, Scherrer constant, wavelength of X-rays and crystallite size, respectively. For this, careful examination of XRD pattern was carried out and the full width at half maximum (FWHM) of major peaks were calculated. From the obtained values, plot between $\beta \cos \theta$ and $\sin \theta$ was drawn and further linearly fitted to obtain strain (η) value from the slope of linearity of data points. The corresponding plot of $\beta \cos \theta$ *vs.* $\sin \theta$ is shown in Fig. 2b. The value of strain (η) for LTP was found out to be $\sim 4.88 \times 10^{-3}$. This value of strain renders an approximate analysis about the presence of point defects in the crystal, which may be further confirmed through high resolution X-ray diffraction (HRXRD). It is interesting to look at the sign of strain, which comes out to be positive and this indicates that crystal may contain interstitial type of defects. In general, the presence of interstitial type of defects in single crystal leads to contraction of the lattice around defect core and hence leads to development of strain in the crystal and the opposite happens when vacancy type defects are present in single crystal, which leads to expansion of lattice around the defect core.[23,24] The presence of interstitial type of defects in LTP crystal was confirmed through HRXRD analysis, which is discussed in the forthcoming section.

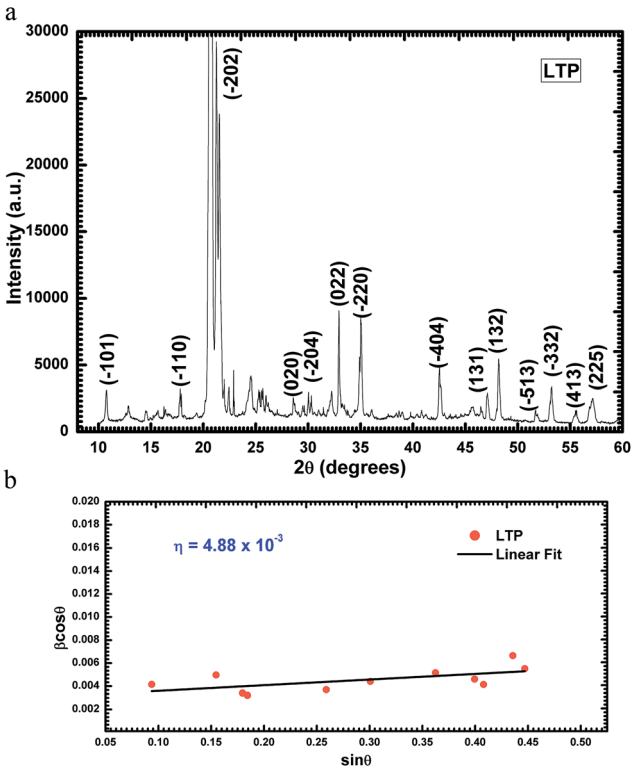

Fig. 2 (a) Powder XRD spectrum of LTP material. (b) Hall Williamson plot for microstrain analysis of LTP.

3.2 Crystalline perfection analysis

Fig. 3 shows the high-resolution diffraction curve (DC) recorded for a typical LTP single crystal specimen using (−202) diffracting planes in symmetrical Bragg geometry with CuKα_1 radiation. As seen in the figure, the DC contains a single peak and indicates that the specimen is free from structural grain boundaries. The full width at half maximum (FWHM) of this curve was 45 arc second, which is slightly more than that expected from the plane wave theory of dynamical X-ray diffraction[25] and revealed the presence of point defects and their aggregates. It is interesting to observe the shape of the DC. The DC was asymmetric with respect to the Bragg peak position. For a particular angular deviation ($\Delta\theta$) of glancing angle (θ) with respect to the Bragg peak position (taken as zero for of convenience), the scattered intensity was considerably more in the positive direction in comparison to that of the negative direction. This feature clearly indicates that the crystal contained predominantly interstitial type of defects than that of vacancy defects. This can be well understood by the fact that due to interstitial defects, the lattice around these defects undergo compressive stress,[26] and the lattice parameter d (interplanar spacing) decreases and leads to give more scattered (also known as diffuse X-ray scattering) intensity at slightly higher Bragg angles (θ_B) as d and $\sin \theta_B$ are inversely proportional to each other in the Bragg equation ($2d \sin \theta_B = n\lambda$; n and λ being the order of reflection and wavelength, respectively, which are fixed). The inset in the curve shows the schematic to illustrate how the lattice around the defect core undergoes compressive stress. The converse explanation is true in case of vacancy defects, which cause tensile stress in the lattice around the

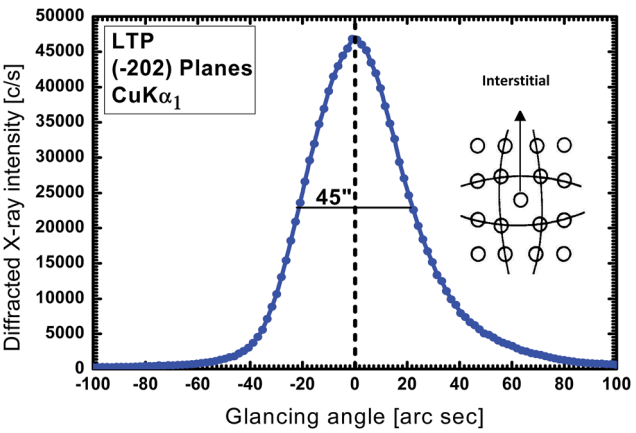

Fig. 3 Diffraction curve recorded for a typical LTP single crystal using (−202) diffracting planes with CuKα_1 radiation. Inset shows the schematic of an interstitial defect.

defect core leading to increase of lattice spacing and in turn results in more scattered intensity at the lower Bragg angles. It may be mentioned here that the variation in lattice parameter is confined very close to the defect core which gives only the scattered intensity close to the Bragg peak. Long range order may not be expected and hence change in the lattice parameter also may not be expected.[27] It may be worth to mention here that the defects were more or less statistically distributed in the crystal. If the defects were not statistically distributed, but distributed here and there as macroscopic clusters leading to mosaic blocks, then the strain generated by such clusters would be larger, leading to cracks and structural grain boundaries, which can be seen very clearly in HRXRD curves with additional peak(s) as observed in our recent study on urea-doped crystals in ZTS at various levels of doping.[28] However, in the present experiments the diffraction curve did not contain any additional peak and indicates the absence of clustering of point defects at macroscopic level. The single diffraction peak with reasonably low FWHM indicates that the crystalline perfection was quite good.

3.3 Optical transmission analysis

Transmission and absorption studies are essential factors to identify a potential NLO material. Crystals to be used for optical applications must possess wide transparency with little absorption in possible electromagnetic spectrum depending on applications as desired. Transmission and absorption spectrum for LTP crystal (shown in Fig. 4a) was recorded in wavelength ranging from 200 to 900 nm. From the curve we observe a wide absorption edge, which leads to higher absorption of lower visible wavelength. This may be because of pale yellow color of the material. This also limits the transmission in lower wavelength visible region from 400 nm to ~471 nm, which also corresponds to cutoff wavelength for this material. But beyond the absorption edge, the crystal exhibits reasonably good transmittance thus favoring its usage for NLO applications. However, the maximum transmittance observed at the edge of the visible region was ~33%, which was lower than expected. This may be because of surface irregularities and scratches as seen from the optical image (Inset to Fig. 4a), which may have occurred while polishing the sample. Moreover, slight disturbance in transmission curve can be seen, which may be due to point defects (interstitial type) in crystal as confirmed from HRXRD analysis described in the previous section. Moreover, almost negligible absorption can be seen in near IR region hence favoring the usage of Nd:YAG laser of wavelength 1064 nm for second harmonic generation (SHG) applications. Further its absorption coefficient was evaluated from the measured transmittance value using

$$\alpha = 2.3026 \log(1/T)/t \quad (7)$$

The calculated absorption coefficient value was used to evaluate the band gap of the material using Tauc relation as

$$\alpha h\nu = A(h\nu - E_g)^{1/2} \quad (8)$$

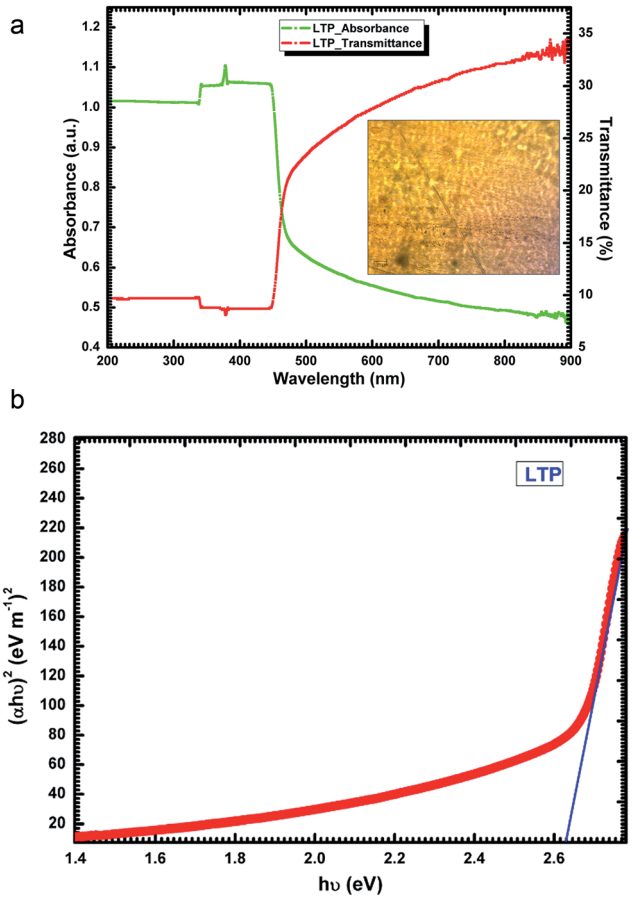

Fig. 4 (a) UV-Vis absorption and transmission spectrum of LTP single crystal. Inset shows the optical image of LTP crystal. (b) Tauc's plot of LTP crystal for band gap evaluation.

The Tauc's plot between $(\alpha h\nu)^2$ and photon energy $(h\nu)$ at room temperature is shown in Fig. 4b. The intercept of straight line on the energy axis gives the value of the band gap to be 2.63 eV thus indicating the material to possess good insulation (dielectric) properties.

3.4 Laser damage threshold measurement

Strength of NLO effect mainly depends on the incident power level, which in turn decides the maximum output power that can be obtained from a given crystal. Thus study of damage threshold for NLO crystals are essential as surface damage by high power laser limits the crystal performance for optical device applications.[29,30] LTP being excellent second harmonic

Table 1 Laser damage threshold of LTP single crystal

	Laser Damage Threshold (LDT) value at 1 pulse per second	
Compound	J cm^{-2}	GW cm^{-2}
L-Threoninium picrate (LTP)	10.2	10.2

generator can be utilized for NLO applications subject to it satisfying other properties, such as large LDT and thermal stability, for electro optical device fabrication. In this regard LDT measurement on 2 mm plate along (−202) plane of LTP crystal was carried out using Nd:YAG laser. The energy density was calculated using the formula E/A where E is the input energy and A is the area of circular spot.[17,18] The value obtained for 1 pulse per second is tabulated in Table 1. LTP was observed to possess reasonably high laser damage threshold value compared to other well-known organic and inorganic crystals, such as KDP and urea, used for NLO applications. This comparison is illustrated in Table 2. This LDT value for LTP crystal is expected to increase with increase in the crystalline perfection, as in present case, as confirmed from HRXRD analysis that crystal possess interstitial type of defect and surface damage was found to be affected by defects in crystal as they act as energy absorbing centers[29] in crystals thus reducing the mechanical strength in the crystal as observed from nano-indentation analysis (explained afterwards). Also specific heat is one of the most important factor, which affects the damage threshold, as a material which possess more specific heat is expected to have smaller temperature gradient thus more resistant to laser damage.[31] Specific heat measured for LTP crystal using PPE technique (discussed in subsequent subsection) clearly gives interpretation about the obtained high damage threshold value for LTP crystal. This higher value of laser damage threshold may be because of strong O–H···O hydrogen bond and a N–H···O hydrogen bond between L-threonine and picric acid. Thus, the obtained higher value of laser damage threshold for LTP crystal clearly makes it a promising candidate for NLO applications.

3.5 Birefringence analysis

Birefringence plays a vital and interesting role in nonlinear optical phenomena and is widely utilized in optical devices like light modulators, liquid crystal displays, crystal filters, and wave plates.[36] One of the main issues of present birefringence analysis was to give an account of how the birefringence measurement associated with optical quality and crystalline perfection of the grown LTP crystal, and for that modified channel spectrum method (MCS) has been employed.[37] During the experiment certain interesting anomalies were observed while using this method with the LTP crystal and the results are explained in detail. In general, a 1000 W quartz iodine lamp (tungsten halogen lamp) was used as the source to illuminate the white light for the dispersion of birefringence measurement. Although, during measurement CCD camera faced difficulties to capture the instantly recognizable fringe patterns of LTP with the above source. This may be due to the pale yellow colour of the LTP crystal (chromic effect), because this colour completely absorbs lower region of visible wavelength (shorter cut off wavelength ~471 nm in transmittance graph). The crystal slightly allows higher wavelength with less intensity to CCD *via* analyzer, which is not only to capture a good quality of fringe pattern, but also to obtain fringe pattern not enough for the accurate dispersion of birefringence measurement. Hence, in the MCS experimental setup, quartz iodine lamp was replaced with high power monochromatic He–Ne laser (λ = 632.8 nm) and used as a source for further dispersion of birefringence analysis. In order to understand further analysis in visible region of electromagnetic spectrum, a series of fringe systems were simulated in a computer using Lab View software. The values of the birefringence have been calculated by first finding the fringe order for particular wavelength and then using the relation:

$$\Delta n = k\lambda/t \quad (9)$$

Table 2 Comparative study of LDT values of LTP crystal with other crystals reported in previously studied reports

Compound	Laser damage threshold (GW cm^{-2})
Potassium dihydrogen phosphate (KDP)	0.2[a,b]
Urea	1.5[a,b]
Imidazolium L-tartrate (IMLT)	7.45[c]
L-Arginine bis(trifluoroacetate) (LATBF)	0.79[d]
BBO	5[e]
L-Prolinium tartrate (LPT)	5.9[f]
L-Arginine phosphate	10[f]
L-Threoninium picrate (LTP)	10.2[g]

[a] Ref. 18. [b] Ref. 32. [c] Ref. 31. [d] Ref. 33. [e] Ref. 34. [f] Ref. 35. [g] Present study.

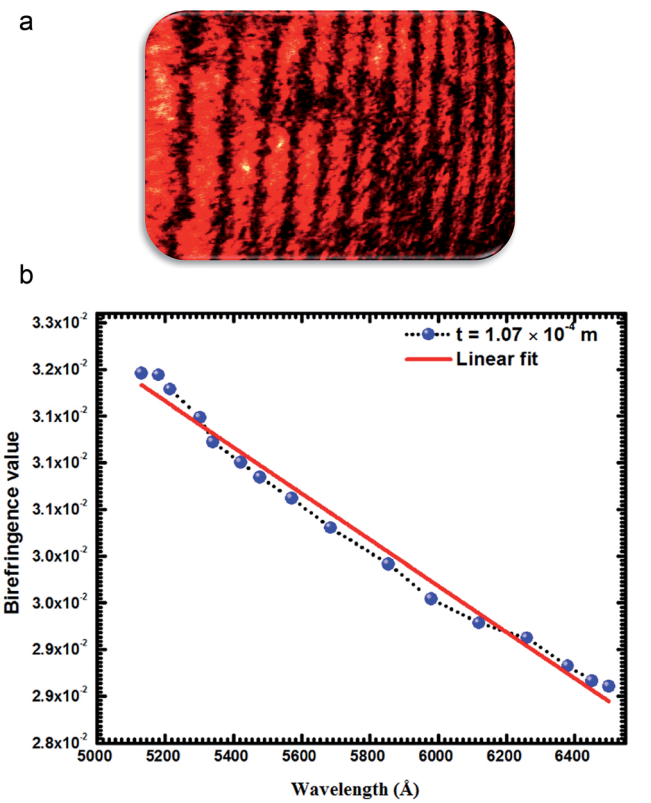

Fig. 5 (a) Birefringence interferogram of LTP single crystal. (b) Birefringence *vs.* wavelength plot of LTP single crystal.

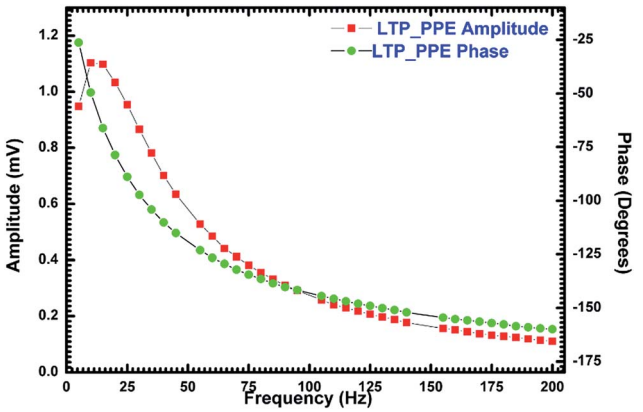

Fig. 6 PPE amplitude and phase *vs.* frequency curve of LTP crystal.

where λ is the wavelength in nm, t is the thickness of the crystal in mm and k is the fringe order.[38] The LTP showed two beam interference fringes and dispersion pattern as shown in Fig. 5a indicating the existence of non uniform symmetry fringes in LTP. Here, we have to consider crystal system of LTP, which was monoclinic. In monoclinic crystal system one of the indicatrix axes always coincide with the crystallographic *b* axis, the other two axes make an angle with crystallographic *a* and *c* axes. The intermolecular and intramolecular interactions, which are hydrogen bonded in LTP, were stronger along the *b*-axis. Correspondingly in the present case, optical linear birefringence values were high in this direction and symmetry dispersion pattern was due to not only the donor–acceptor strength (which is considerably high) but also because of linear zigzag head-to-tail chain of L-threonine.[2] The graph drawn between birefringence ∇n and wavelength (λ) is represented in Fig. 5b. The birefringence value of the grown LTP crystals was found to be 0.0289 at the wavelength 632.8 nm for the thickness of 107 μm. When a crystal was used in a harmonic generation or parametric oscillation device, it is necessary for the crystal to have a relatively large birefringence because this causes wide range phase matching. However, the converting efficiency of the laser in harmonic generation was lowered as the birefringence of the crystal became larger. Therefore, if the crystal is used only in harmonic generation device with a particular wavelength range, only the minimum birefringence of the crystal which causes phase matching is required. The low birefringence value ($\Delta n = 0.0289$ at $\lambda = 632.8$ nm) indicates that the LTP crystal is suitable for harmonic generation device. The obtained values were found to be positive integers and decrease with increasing wavelength, which illustrates that the grown LTP possessed negative dispersion of birefringence and was optically positive at room temperature. The negative dispersion in materials can be utilised for development of a pair of prisms for the production of a net negative dispersion, hence providing a way to help in balancing the positive dispersion of the laser medium.[39] Dispersion of birefringence value play an immense role in many optical applications, which require usage of crystals like in design and development of retardation plates, polarizers *etc.* However, when it comes to harmonic generation applications smaller dispersion in birefringence favours fair conversion efficiency.[40] The plot (Fig. 5b) depicts some distortions from the linearity curve, which may be due to the point defects in the specimen and is in tune with HRXRD analysis. The birefringence interferogram plays an immense role in determination of optical homogeneity and defects in the crystals.[41] The interferogram of LTP crystal shows non uniform fringe widths thus giving sign of slight non homogeneity inside the crystal which may be because of the presence of interstitial type of defects as supported by diffraction (rocking) curve described in previous section. This was also confirmed from slight disturbance in the visible region of transmittance curve.

3.6 Measurement of thermal parameters

Owing to its excellent second order nonlinear optical properties, LTP crystal may be employed for a wide variety of optical applications. However, a crystal has good nonlinear optical properties only may not fulfill the criteria for its utilization for any particular application, as nonlinear optical properties also depend on the intensity of input laser beam. The higher the

Table 3 Comparative analysis of thermal parameters of LTP crystal with other crystals reported in the literature

Sample	Thermal diffusivity, α ($\times 10^{-6}$ m^2 s^{-1})	Thermal effusivity, e (Wm^{-2} K^{-1} s$^{+1/2}$)	Specific heat capacity, C_p (J kg^{-1} K^{-1})	Thermal conductivity, K (W mK^{-1})
Allylthiourea cadmium bromide (ATCB)[a]	6.47 ± 0.39	3122 ± 62	776 ± 20	7.93 ± 0.37
Allylthiourea cadmium chloride (ATCC)[a]	5.27 ± 0.28	1196 ± 65	101.1 ± 18	8.8689 ± 0.40
$LiNbO_3$ (LN)[b,c]	—	—	648 (300 K)	4.60 (300 K)
$LiIO_3$[c]	—	—	365	1.47
KDP[b]	—	—	857	1.21
Barium Titanate (BT)[b]	—	—	439	1.34
GaAs[b]	—	—	318	52
BBO[b]	—	—	490	1.6
L-Threoninium picrate (LTP)[d]	1.35 ± 0.68	769 ± 12	580 ± 9	0.89 ± 0.02

[a] Ref. 43. [b] Ref. 42. [c] Ref. 44. [d] Present study.

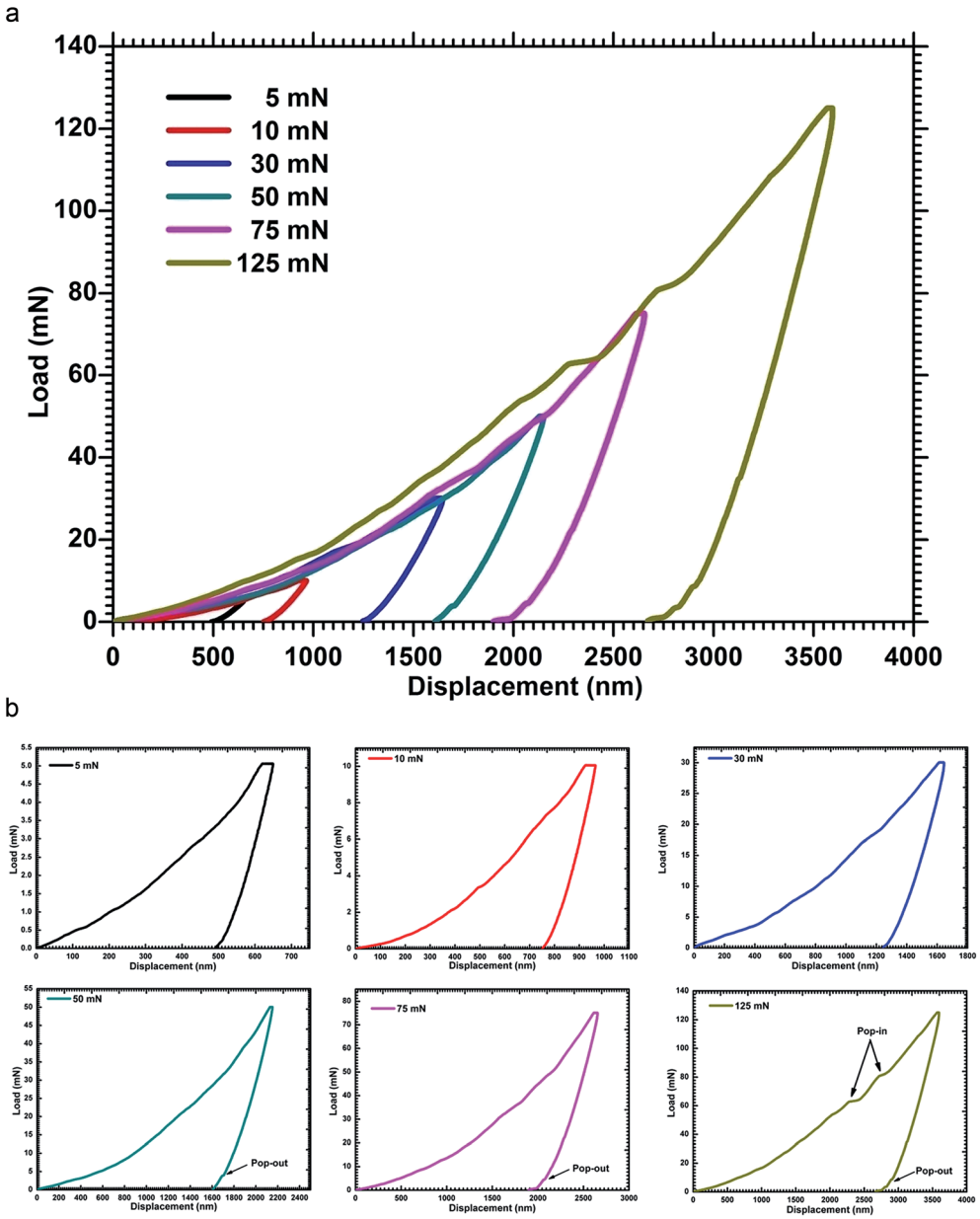

Fig. 7 (a) Load-displacement curve on the LTP single crystal along (−202) plane. (b) Expanded view of load-displacement curve on the LTP single crystal at each load along (−202) plane.

intensity of input optical wave, the higher the nonlinear effect is; the laser intensity is given by

$$I = \frac{P}{A} \tag{10}$$

where P is the power of the input beam and A is the area of cross section of the beam. So the incident intensity can be increased either by increasing the power of the laser beam or by focusing same power into a smaller cross-sectional area. However, there is a limit to increase the strength of the laser beam as it may often lead to the damage of the crystal, which was determined by the value of laser damage threshold of the crystal. Moreover, as the beam passes through the crystal, absorption also occurs, leading to generation of heat inside the crystal. As the crystals are generally anisotropic, this absorption leads to development of temperature gradients inside them, which sometimes results in the generation of cracks. This non-uniform temperature

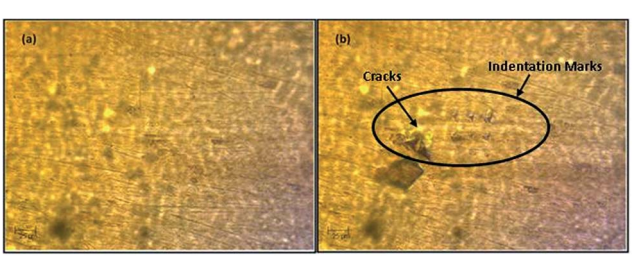

Fig. 8 Optical image of LTP single crystal along (−202) plane (a) before and (b) after indentation.

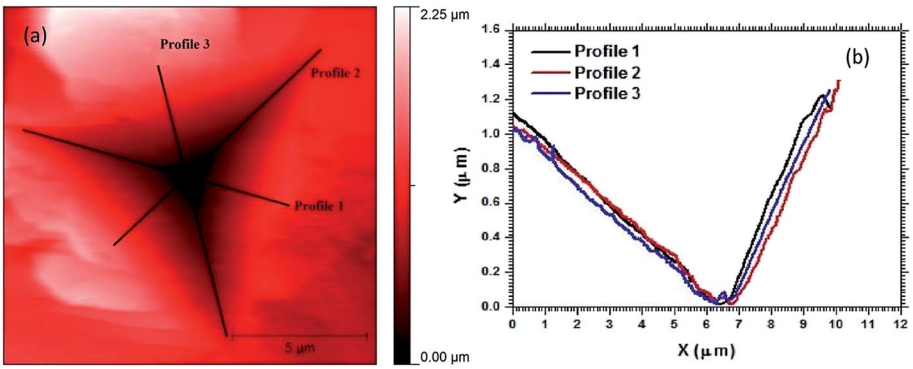

Fig. 9 (a) AFM topography image, indicating imprint made after indentation along (−202) plane of LTP. (b) Depth profile of the indentation imprint after applying 30 mN load.

Table 4 Various obtained parameters associated with the mechanical property of LTP single crystal along (−202) plane

F (mN)	Hit (Mpa)	Hv (Vickers)	Eit (Gpa)	hm (nm)	S [mN nm^{-1}]	hc (nm)	hr (nm)	hp (nm)	Ap (nm^2)	m
5.053	633.047	58.627	13.435	649.778	0.048	570.076	544.612	496.016	7 982 329	1.413
10.048	557.3	51.612	13.039	965.222	0.07	856.786	821.899	755.465	18 030 548	1.427
30.039	595.309	55.132	11.987	1644.242	0.108	1433.301	1365.923	1255.392	50 459 012	1.412
50.054	571.685	52.944	11.983	2151.417	0.142	1888.033	1799.251	1611.016	87 555 400	1.53
75.045	560.04	51.866	11.938	2654.148	0.175	2335.719	2225.763	1969.022	134 000 064	1.595
125.065	501.828	46.475	11.409	3593.828	0.228	3185.367	3046.338	2747.51	249 219 856	1.556

gradient also has adverse effects on beam profile and phase fronts. It is known that the higher the specific heat of a crystal, the smaller the temperature gradient will be. This minimizes the chances of formation of cracks in the crystal.[42] Thus measurement and analysis of thermal parameters like specific heat and thermal conductivity provide information about thermal stability and limit up to which the crystal can withstand the power of high energy laser pulses. In this regard thermal analysis on LTP crystal was carried out using PPE technique, using which PPE amplitude and phase curve *vs.* frequency were obtained (shown in Fig. 6) and various thermal parameters were evaluated using these curves.

From the values tabulated in Table 3 we observe that LTP crystal possess a better thermal stability on account of the fact that it possess comparatively high specific heat capacity, which is highly desirable for it to be used for NLO applications. A high value for specific heat also means a high value for the laser damage threshold for the crystal. Furthermore, a comparison of thermal properties of several known organic and inorganic crystals with those of LTP crystal has been carried out by us, and these values are also tabulated in Table 3. From the table we see that LTP possess higher specific heat capacity than the well-known BBO and GaAs single crystals, but is lower than $LiNbO_3$, ATCB or KDP single crystals. It can also be noticed from Table 3 that thermal conductivity of LTP is lower than most other organic or inorganic crystals reported in previously studied methods. Thus, though LTP crystal possess high specific heat favouring resistance to laser damage, its low thermal conductivity prevents conduction of accumulated heat away from it, which is not desirable from the point of view of laser damage threshold. The low thermal conductivity effectively lowers the laser damage threshold of the material. This limitation can to a great extent be overcome by suitably fixing the crystal on to a thermally conducting substrate.

3.7 Mechanical stability analysis

Crystal to be used for photonics application should not only possess better optical properties but also at the same time should be able to withstand the effect high power laser *i.e.* they

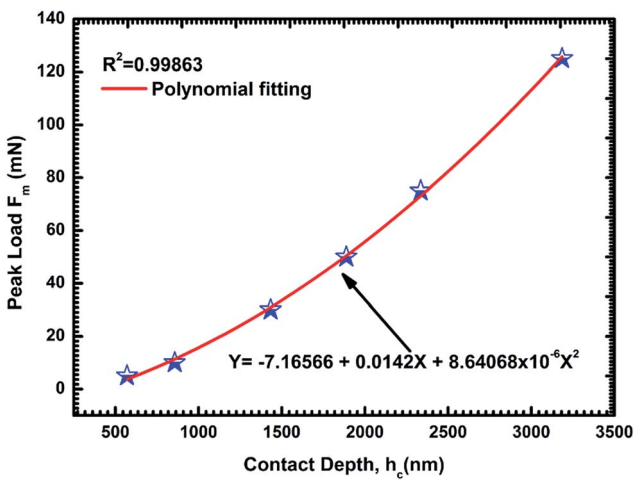

Fig. 10 Variation of contact depth with peak load for LTP crystal.

should possess high resistance to laser damage. Resistance to laser damage also depends on the mechanical stability in the crystals, which in turn depends on various mechanical properties of crystal like hardness, stiffness *etc.* Nanoindentation is an excellent technique for evaluating the mechanical properties of material on nanoscale hence in the present work nanoindentation analysis was carried out on LTP single crystal. Fig. 7a represents the load displacement curve as obtained from (−202) plane of LTP crystal using the procedure described in experimental section. From the detailed analysis of the curve we may say that LTP is softer than inorganic quartz and sapphire crystal[22] with peak depth at maximum load of ~2740 nm, this may be due to the organic nature of the materials as they possess moderate mechanical stability. Moreover, on careful examination of the curve at each load (Fig. 7b) we found that there was a slight appearance of pop-in(s) in curve from 10 to 75 mN, which happens when there is transformation from elastic to elastic/plastic region due to nucleation of plastic deformation owing to defects in single crystals such as dislocations, point defects and cracks.[45] The presence of point defect (interstitial type) was observed from our HRXRD analysis, which may be one of the reasons for the occurrence of plastic deformation in crystal. However, strong visibility of pop-in can be seen at peak load of 125 mN, indicating the occurrence of cracks in the crystal, which can be observed from optical image (shown in Fig. 8b) of the crystal after indentation. This formation of crack at the surface on LTP crystal may be because of high value of strain offered by Berkovich tip compared to Vickers and other indenters leading to higher stress in deformed region.[45] At peak load from 50 to 125 mN pop-out(s) can also be seen, which generally occurs because of sudden change in volume due to pressure induced phase transformation.[46]

Fig. 9a and b show good correlation between nanoindentation depth profile and profile obtained from AFM image at load of 30 mN. Further load displacement curve was analysed and various mechanical parameters were evaluated in accordance with the eqn (1) to (5) described in experimental section. These parameters are listed in Table 4. From the table we observe there is decrease in the value of hardness and young's modulus as the load is increased from 5 to 125 mN. This decrease in value may be attributed to indentation size effect.[44] From Fig. 10 we observe the increment in contact depth with peak load this may be because of decrease in hardness of LTP with load. Moreover, as the contact depth (h_c) and peak load (F_m) are related as,

$$F_m = a_o + a_1 h_c + a_2 h_c^2 \quad (11)$$

Thus the plot of contact depth *vs.* peak load was fitted with using polynomial function and the value of a_2, which is considered as a measure of load independent hardness, was found to be 8.64068×10^{-6} mN nm^{-2}. Further using eqn (5) load independent hardness (H_0) was found to be 352.68 MPa. This value of H_0 was more than the hardness of a recently reported[47] organic L-prolinium tartrate (LPT) single crystal thus indicating that LTP crystal possess more ability to resist deformation.

Further Young's modulus of LTP crystal was plotted with load (shown in Fig. 11), which indicates a decrease in its value with load and it may be because of increase in strain in crystal due to the load offered by much sharper Berkovich tip. Fig. 12 shows the variation of stiffness with contact depth. A linear relation was observed between them, which is in accordance with equation given as,

$$S = a + bh_c \quad (12)$$

where a and b are constants related to indenter tip rounding and reduced Young's modulus. The slope (b), which indicates the reduced Young's modulus, was found from the linear fit of this curve to be 6.9229×10^{-5} mN nm^{-2} or 69.22 GPa. Moreover, constant b, which is an intercept, was found to be 0.01. If

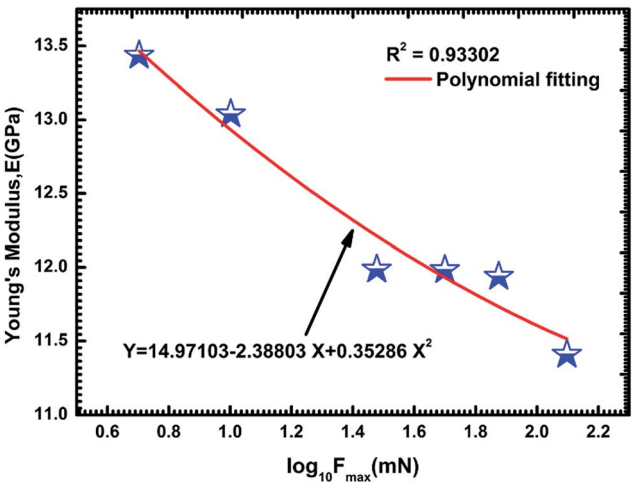

Fig. 11 Variation of Young's modulus extracted from the analysis of the load-displacement curves as a function of peak load along (−202) plane of LTP crystal.

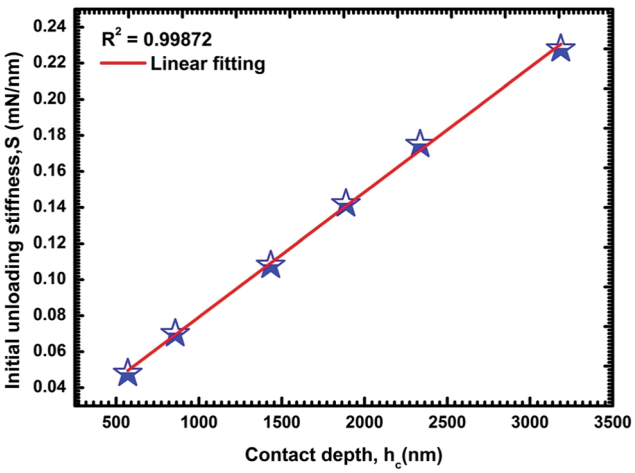

Fig. 12 Variation of initial unloading stiffness (S) with the contact depth at peak load for LTP crystal.

there would be best linear fit this value of b, which is due to indenter tip rounding, would not have occurred. Thus overall we may conclude that LTP single crystal possess moderate mechanical properties such as hardness and Young's modulus.

4. Conclusions

Bulk single crystal of L-threoninium picrate an excellent material for electro-optic applications was successfully grown by conventional slow evaporation solution technique. The powder XRD analysis confirmed its crystal system and space group and that is in good coincidence with reported studies. Strain was evaluated using Hall–Williamson's relation and indicated the presence of interstitial type of defect in crystal, which was further correlated with crystalline perfection analysis results. HRXRD analysis revealed that crystalline perfection of LTP crystal was fairly good; however, interstitial type of defect was found to exist. Optical transmission and absorption analysis confirmed large absorption edge, which may be because of the pale yellow color of LTP material but beyond 471 nm the crystal was found to be transparent, thus favouring its usage for optical applications. Laser damage threshold studies revealed that the crystal possess significantly large value of damage threshold than many of the organic single crystals reported in previously studied reports. This value was also in accordance with large specific heat of LTP crystal as obtained from PPE analysis. Low birefringence of LTP obtained using modified channel spectrum method confirmed the usage of LTP crystal for harmonic generation applications; however, there was slight disturbance in optical homogeneity as indicated from interferogram. Thermal analysis confirmed that LTP crystal possess relatively large specific heat compared to other crystals, thus providing a correlation with the obtained large laser damage threshold value. Mechanical analysis indicates that the crystal possess moderate mechanical properties; however, its load independent hardness was found to be higher than the recently reported L-prolinium tartrate single crystal. Thus, overall LTP crystal possess better optical, thermal and mechanical properties compared to many well-known organic crystals, hence favouring its usage for NLO applications.

Acknowledgements

The authors' are highly obliged to thank the Director Prof. R. C. Budhani, CSIR-NPL for his continuous encouragement and support in carrying out the present work. One of the author Anuj Krishna is highly thankful to CSIR for giving financial assistance. Budhendra Singh would like to express his personal thanks to FCT (Fundaçãopara a Ciência e a Tecnologia) for post-doctoral research grants with reference numbers SFRH/BPD/76184/2011.

References

1 S. K. Kushwaha, M. Shakir, K. K. Maurya, A. L. Shah, M. A. Wahab and G. Bhagavannarayana, *J. Appl. Phys.*, 2010, **108**, 033506–0033512.
2 S. Natarajan, M. Umamaheswaran, J. Kalyana Sundar, J. Suresh and S. A. M. B. Dhas, *Spectrochim. Acta, Part A*, 2010, **77**, 160–163.
3 D. W. Chen and J. J. Yeh, *Opt. Lett.*, 1988, **13**(10), 808–810.
4 G. D. Boyd, R. C. Miller, K. Nassau, W. L. Bond and A. Savage, *Appl. Phys. Lett.*, 1964, **5**(11), 234–236.
5 C. Chen, Y. Wu, A. Jiang, B. Wu, G. You, R. Li and S. Lin, *J. Opt. Soc. Am. B*, 1989, **6**(4), 616–621.
6 G. R. Kumar, S. G. Raj, R. Mohan and R. Jayavel, *Cryst. Growth Des.*, 2006, **6**(6), 1308–1310.
7 S. Suresh, A. Ramanand, D. Jayaraman and P. Mani, *Rev. Adv. Mater. Sci.*, 2012, **30**, 175–183.
8 G. Dematos, V. Venkataraman, E. Nogueria, M. Belsley, P. A. Criado, M. J. Dianez and E. P. Garrido, *Synth. Met.*, 2000, **115**, 225–228.
9 S. A. M. B. Dhas, G. Bhagavannarayana and S. Natarajan, *J. Cryst. Growth*, 2008, **310**, 3535–3539.
10 P. Srinivasan, T. Kanagasekaran, R. Gopalakrishnan, G. Bhagvannarayana and P. Ramasamy, *Cryst. Growth Des.*, 2006, **6**, 1663–1670.
11 J. Oudar and R. Hierle, *J. Appl. Phys.*, 1977, **48**, 2699–2704.
12 K. C. Bright and T. H. Freeda, *Phys. B*, 2010, **405**, 3857–3861.
13 D. Kalaiselvi, R. M. Kumar and R. Jayavel, *Cryst. Res. Technol.*, 2008, **43**(8), 851–856.
14 K. Thukral, N. Vijayan, B. Rathi, G. Bhagavannaryana, S. Verma, J. Philip, A. Krishna, M. S. Jeyalakshmy and S. K. Halder, *CrystEngComm*, 2014, **16**, 2802–2809.
15 H. S. Nalwa, T. Watanabe and S. Miata, in *Nonlinear Optics of Organic Molecules and Polymers*, ed. H. S. Nalwa and S. Miata, CRC Press, New York, 1997, p. 120.
16 G. Bhagavannarayana and S. K. Kushwaha, *J. Appl. Crystallogr.*, 2010, **43**, 154–162.
17 N. Rani, N. Vijayan, B. Riscob, S. K. Jat, A. Krishna, S. Dhas, G. Bhagvannarayana, B. Rathi and M. A. Wahab, *CrystEngComm*, 2013, **15**, 2127–2132.
18 S. A. M. B. Dhas, G. Bhagavannarayana and S. Natarajan, *Open Crystallogr. J.*, 2008, **1**, 42–45.
19 K. Thukral, N. Vijayan, B. Rathi, G. Bhagavannaryana, S. Verma, J. Philip, A. Krishna, M. S. Jeyalakshmy and S. K. Halder, *CrystEngComm*, 2014, **16**, 2802–2809.
20 C. P. Menon and J. Philip, *Meas. Sci. Technol.*, 2000, **11**, 1744–1749.
21 A. C. F. Cripps, *Surf. Coat. Technol.*, 2006, **200**, 4153–4165.
22 W. C. Oliver and G. M. Pharr, *J. Mater. Res.*, 1992, **7**(6), 1564–1583.
23 B. Riscob, R. Bhatt, N. Vijayan, I. Bhaumik, S. Ganesamoorthy, M. A. Wahab, Rashmi and G. Bhagavannarayana, *J. Appl. Crystallogr.*, 2013, **46**, 601–609.
24 S. K. Kushwaha, K. K. Maurya, N. Vijayan, B. Kumar, R. Bhatt, S. Ganesamoorthy and G. Bhagavannarayana, *CrystEngComm*, 2012, **14**, 3297–3305.
25 B. W. Batterman and H. Cole, *Rev. Mod. Phys.*, 1964, **36**, 681–717.
26 G. Bhagavannarayana, S. Parthiban and S. Meenakshisundaram, *Cryst. Growth Des.*, 2008, **8**, 446–451.

27 G. Bhagavannarayana, S. K. Kushwaha, M. Shakir and K. K. Maurya, *J. Appl. Crystallogr.*, 2010, **44**, 122–128.
28 G. Bhagavannarayana and S. K. Kushwaha, *J. Appl. Crystallogr.*, 2010, **43**(1), 154–162.
29 S. Vanishri, H. L. Bhat, A. Deepthy, V. P. N. Nampoori, E. de Matos Gomes and M. Belsley, *J. Appl. Phys.*, 2006, **99**, 083107–083111.
30 N. L. Boling, M. D. Crisp and G. Dube, *Appl. Opt.*, 1973, **12**, 650–660.
31 C. Ji, T. Chen, Z. Sun, Y. Ge, W. Lin, J. Luo, Q. Shi and M. Hong, *CrystEngComm*, 2013, **15**, 2157–2162.
32 N. Vijayan, G. Bhagavannarayana, K. R. Ramesh, R. Gopalakrisnan, K. K. Maurya and P. Ramasamy, *Cryst. Growth Des.*, 2006, **6**, 1542–1546.
33 Z. Sun, G. Zhang, X. Wang, Z. Gao, X. Cheng, S. Zhang and D. Xu, *Cryst. Growth Des.*, 2009, **9**(7), 3251–3259.
34 R. S. Adhav, S. R. Adhav and J. M. Pelaprar, *Laser Focus*, 1987, **23**, 88.
35 S. A. M. B. Dhas and S. Natarajan, *Cryst. Res. Technol.*, 2007, **42**(5), 471–476.
36 P. Krishnan, K. Gayathri, P. R. Rajakumar, V. Jayaramakrishnan, S. Gunasekaran and G. Anbalagan, *Spectrochim. Acta, Part A*, 2014, **131**, 114–124.
37 G. Bhoopathi, V. Jayaramakrishnan, K. Ravikumar, T. Prasanyaa and S. Karthikeyan, *Mater. Sci.-Pol.*, 2013, **31**, 1–5.
38 P. Krishnan, K. Gayathri, G. Bhagavanarayana, V. Jayaramakrishnan, S. Gunasekaran and G. Anbalagan, *Spectrochim. Acta, Part A*, 2013, **112**, 152–160.
39 R. L. Fork, O. E. Martinez and J. P. Gordon, *Opt. Lett.*, 1984, **9**, 150–152.
40 A. L. Bajor, T. Piatkowski and M. Lesniewski, *Meas. Sci. Technol.*, 2006, **17**, 427–435.
41 K. Sangeetha, R. Ramesh Babu, G. Bhagavannarayana and K. Ramamurthi, *Mater. Chem. Phys.*, 2011, **130**, 487–492.
42 S. Manivannan, S. Dhanuskodi, S. K. Tiwari and J. Philip, *Appl. Phys. B*, 2008, **90**, 489–496.
43 G. Sreekanth, P. Thomas, S. Chandralingam, M. Augustine, S. George and G. P. Joseph, *IOP Conf. Ser.: Mater. Sci. Eng.*, 2013, **43**, 012007, DOI: 10.1088/1757–899x/43/1/012007.
44 S. K. Jat, N. Vijayan, A. Krishna, J. Philip, S. Verma, I. Bdikin, B. Singh, G. Bhagavannarayana and S. K. Halder, *CrystEngComm*, 2013, **15**, 10034–10042.
45 I. Bdikin, B. Singh, J. S. Kumar, M. P. F. Graca, A. M. Balbashov, J. Grácio and A. L. Kholkin, *Scr. Mater.*, 2014, **74**, 76–79.
46 U. Ramamurty and J. Jang, *CrystEngComm*, 2014, **16**, 12–23.
47 K. Thukral, N. Vijayan, B. Singh, I. Bdikin, D. Haranath, K. K. Maurya, J. Philip, H. Soumya, P. Sreekanth and G. Bhagavannarayana, *CrystEngComm*, 2014, **16**, 9245–9254.